THE JOURNAL OF PHYSICAL CHEMISTRY B

Article

pubs.acs.org/JPCB

Investigations of the Very Short Hydrogen Bond in the Crystal of Nitromalonamide via Car−Parrinello and Path Integral Molecular Dynamics

Piotr Durlak,* Krzysztof Mierzwicki, and Zdzisław Latajka

Faculty of Chemistry, University of Wrocław, 14 F. Joliot-Curie Street, 50-383 Wrocław, Poland

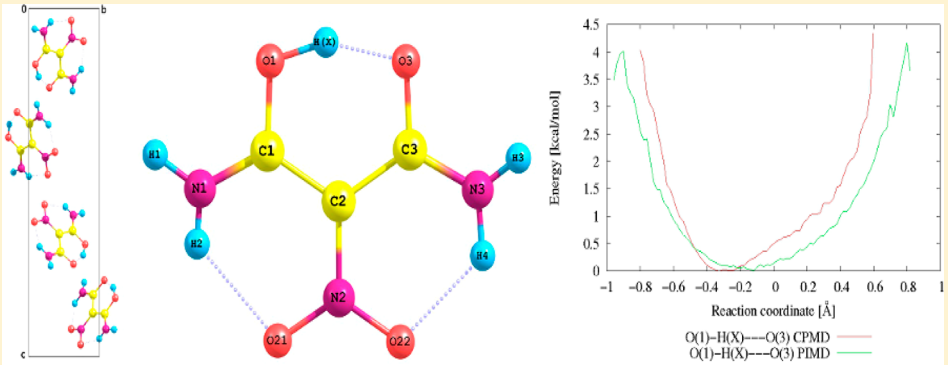

ABSTRACT: In this paper are presented the results of theoretical studies of the structure in proton motion in a very short O···O and two weak N−H···O intramolecular hydrogen bonds in the nitromalonamide crystal. The dynamics of proton motion in hydrogen bonds were investigated in the NVT ensemble at 298 K using the Car−Parrinello and the path integral molecular dynamics. A very large delocalization of proton in the slightly asymmetrical single well of free energy potential of O−H···O intramolecular hydrogen bond was noted especially in the path integral simulation where quantum effects are taken into account. This hydrogen bond is very strong with the estimated energy of hydrogen bond ca. −27 kcal/mol. The nature of intra- and intermolecular interactions was studied by means of quantum theory of atoms in molecules. The infrared spectra were calculated and compared with available experimental data. CPMD vibrational results appear to be in good agreement with the experimental ones.

INTRODUCTION

Hydrogen-bonded systems play a very important role in many physical, chemical, and biological processes.[1−10] The most interesting and important systems are those with strong hydrogen bonds (H-bonds). More than twenty years ago Gilli and co-workers, in order to explain the appearance of strong and very strong intra- and intermolecular H-bonds in some molecular systems, introduced the concept of resonance-assisted hydrogen bond (RAHB), where the H-bond donor and acceptor are connected through π-conjugated double bonds.[10−15] A few good examples of resonance-assisted hydrogen-bonded complexes are β-diketones and other similar systems. Due to π-delocalization within the O═C−C═C−O−H keto−enol chelate ring the equalization of C═O and C−C as well as C═O and C−O bond lengths is noted.[10] Therefore it has been suggested that hydrogen bond strength depends on the degree of resonance within the π-conjugated double bonds. Moreover, due to the consequences of π-electron delocalization, the intramolecular H-bonds are characterized by shortening the length of the O···O intermolecular bond up to 2.4 Å, or even less, and the strengthening of the H-bond and proton being shifted toward the center of the O···O bond.[10]

The resonance-assisted character of intramolecular hydrogen bonding was also proved in heterocyclic molecules.[16−18] It was shown that the position of tautomeric equilibrium is controlled by the aromaticity of the heterocycle, which is different for two tautomers, and relative proton affinities of two heteroatoms involved in the intramolecular H-bond formation.[18] Several review papers were published about RAHB.[10,19−22]

In recent years, much attention has been paid to the studies of keto−enol tautomerism and proton transfer in the enol tautomer of malonaldehyde and its derivatives (for example, see refs 23−32). Due to the intramolecular H-bond the enol form exists only in the solid state and is also more stable than the keto one. However, the keto−enol equilibrium is also observed in solvents. An interesting member of this group of compounds, which belongs to the RAHB, is nitromalonamide (NMA), presented in Figure 1. NMA is an unusual example of molecular system with three intramolecular hydrogen bonds of different strengths. One of them, the O−H···O intramolecular hydrogen bond, is very short. The experimental value of the O···O

Received: December 18, 2012
Revised: April 10, 2013

dx.doi.org/10.1021/jp312473b | J. Phys. Chem. B XXXX, XXX, XXX−XXX

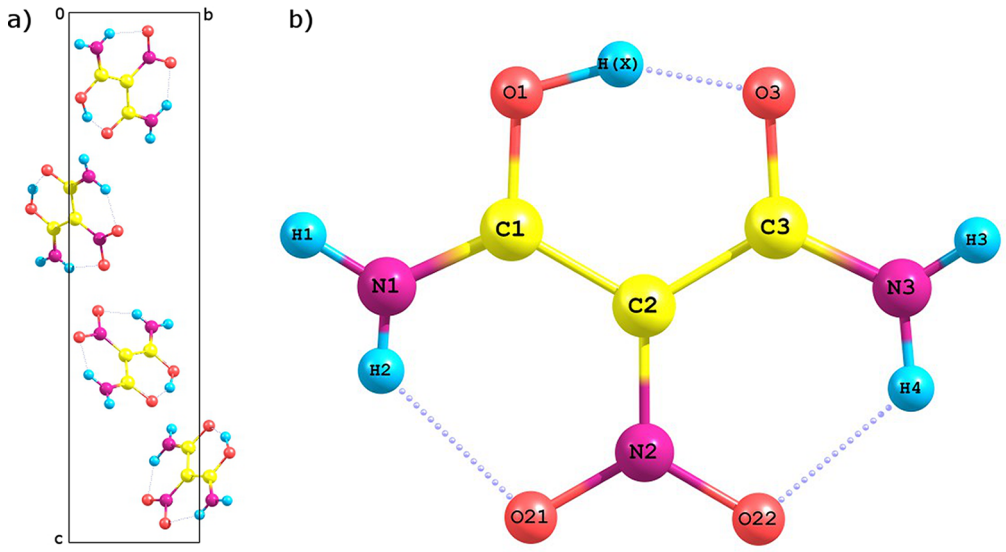

Figure 1. The crystal structure of nitromalonamide (a); the drawing of nitromalonamide showing the numbering of atoms (b).

distance of NMA crystal obtained from the X-ray analysis is 2.384 Å[33] and from the neutron diffraction at 15 K gives this distance of 2.391 Å.[34] It means that this intramolecular O−H···O hydrogen bond is one of the shortest hydrogen bonds between oxygen atoms. The enol hydrogen in the crystal is asymmetrically located between the two oxygen atoms with distances of 1.14 Å for the O−H bond and 1.31 Å for the H···O contact.[34] The other two hydrogen bonds of (H)N−H···O(N) type are much longer and are the result of interaction between an amino hydrogen atom and an oxygen atom of the nitro group. All three intramolecular hydrogen bonds make the molecule planar and increase the chelate ring conjugation with consequent strengthening of the O−H···O bridge. Moreover, the oxygen atoms of the C═O groups form the intermolecular hydrogen bonds with one of the hydrogen atoms of the NH_2 groups. Theoretical calculations of Buemi and Zuccarello of NMA in vacuo indicate that the strength of the short O−H···O hydrogen bond is ca. 27 kcal/mol.[35,36] Furthermore, on the basis of ab initio calculations they indicated an important role of the two (H)N−H···O(N) intramolecular hydrogen bonds which make strengthen the O−H···O interaction in NMA with respect to malonamide.

Early theoretical studies on the NMA molecule in vacuum found the potential for proton transfer to be a double minimum (C_s symmetry) with a barrier height of 0.6 and 1.2 kcal/mol, depending on the used theoretical method, and with a structure of C_{2v} being in a transition state.[33] Later studies of Hargis and co-workers on a high level of theory confirmed the symmetric double well potential of proton motion in the O−H···O intramolecular H-bond in the gas phase with a barrier of 0.43 kcal/mol.[29]

Madsen and co-workers to investigate the influence of crystal environment used a very simple model in which the central NMA molecule was placed in the electrostatic potential generated by a set of Mulliken charges at the atomic positions of nearest neighbors.[34] The calculations at the B3LYP/cc-pVDZ level show that the symmetrical double well potential disappeared. The mirrored C_s structure has an energy of 0.23 kcal/mol higher than the original C_s structure. Therefore, it was concluded that the asymmetry of the O−H···O hydrogen bond results from the influence of the crystal environment. This suggestion was supported by studies of deuterium isotope effects on ^{13}C chemical shift which suggest that in solution the two C_s structures will be in equilibrium.[37] Sebban et al. studied ^1H, ^{13}C, and ^{15}N NMR spectra of nitromalonamide and found an enol form and keto form in the ratio 55:45.[38]

The main goal of this paper was the systematic theoretical studies of properties and hydrogen bond dynamics in the nitromalonamide crystal. The standard "static" ab initio calculations are very useful to obtain the information of the localization of critical points (minima and transition state structures) on the potential energy surface (PES). However, hydrogen-bonded systems are not static but fluctuate on the femtosecond ultrashort time scale.[6] Therefore we decided to use molecular dynamics approaches. From a theoretical perspective the accurate modeling of proton transfer dynamics in hydrogen-bonded systems is a challenging problem. Bond formation and breaking due to the proton transfer are not described correctly by conventional molecular mechanics force field. Therefore in this paper two types of molecular dynamics simulations were carried out. First, the behavior of all atoms was treated classically within the Car−Parrinello (CPMD) formalism.[39] Second, the path integral molecular dynamics (PIMD) was applied.[40−42] Within the PIMD approach it is possible to obtain more reliable description of nuclear motion due to the quantum effects incorporated in the simulations. It maps the problem of a quantum particle into one of a classical ring polymer model with N beads that interact through temperature and mass dependent spring forces. In practice, the representation of each atom in the system as a group of N beads requires N electronic structure calculations, and therefore requires much larger computational expense than CPMD. All simulations were carried out for a crystal at 298 K.

Moreover, an additional goal of this paper was a characterization of all intra- and intermolecular hydrogen bonds existing in the NMA crystal by means of the Bader theory of atoms in molecules (AIM).[43]

CALCULATION DETAILS

The calculations of static properties for the NMA crystal were performed with the CRYSTAL09 program.[44,45] Full geometry optimization of the crystal (geometrical parameters and crystal

dx.doi.org/10.1021/jp312473b | J. Phys. Chem. B XXXX, XXX, XXX−XXX

Table 1. Calculated Selected Geometrical and Cell Parameters after Optimization Compared with the Average Geometrical Parameters from CPMD (Standard Deviation in Parentheses) and Existing Experimental Data for the Nitromalonamide in the Solid State[a]

bonds [Å]	PBE	PBE+D[b]	PCG	CPMD	expt[c]
O(1)−O(3)	2.391	2.390	2.399	2.419 (0.059)	2.391
O(1)−H(X)	1.084	1.087	1.114	1.150 (0.106)	1.140
O(3)−H(X)	1.349	1.347	1.327	1.324 (0.135)	1.308
O(1)−C(1)	1.315	1.316	1.317	1.317 (0.027)	1.292
O(3)−C(3)	1.291	1.291	1.289	1.297 (0.027)	1.285
O(21)−N(2)	1.263	1.263	1.260	1.261 (0.023)	1.256
O(22)−N(2)	1.271	1.270	1.254	1.261 (0.024)	1.258
C(1)−C(2)	1.459	1.458	1.449	1.455 (0.031)	1.466
C(2)−C(3)	1.476	1.473	1.473	1.473 (0.033)	1.463
C(1)−N(1)	1.327	1.325	1.327	1.331 (0.024)	1.317
C(2)−N(2)	1.398	1.359	1.420	1.428 (0.032)	1.394
C(3)−N(3)	1.476	1.333	1.332	1.332 (0.024)	1.323
N(1)−H(1)	1.026	1.027	1.026	1.027 (0.027)	1.011
N(1)−H(2)	1.028	1.028	1.026	1.030 (0.027)	1.021
N(3)−H(3)	1.029	1.028	1.024	1.033 (0.027)	1.026
N(3)−H(4)	1.025	1.026	1.025	1.028 (0.027)	1.025
O(21)···H(2)	1.872	1.868	1.930	1.915 (0.119)	1.897
O(22)···H(4)	1.821	1.812	1.853	1.868 (0.118)	1.851

cell [Å]	PBE	PBE+D[b]	expt[c]
a	4.885	4.729	4.842
b	4.995	4.993	4.967
c	23.909	21.389	21.899

angles [deg]	PBE	PBE+D[b]	PCG	CPMD	expt[c]
O(1)−H(X)−O(3)	158.3	158.1	158.5	156.2 (5.4)	155.1
C(1)−O(1)−H(X)	104.2	104.4	103.3	103.5 (3.6)	105.9
C(3)−O(3)−H(X)	102.7	102.8	102.7	103.0 (3.4)	104.7
O(1)−C(1)−C(2)	118.3	118.2	118.5	118.7 (2.6)	117.8
O(1)−C(1)−N(1)	117.2	117.8	116.2	116.4 (3.0)	117.7
C(2)−C(1)−N(1)	124.4	123.9	125.2	124.5 (3.1)	124.4
C(1)−C(2)−C(3)	117.9	118.1	118.4	118.4 (2.4)	118.7
C(1)−C(2)−N(2)	120.3	120.3	120.3	120.4 (2.5)	120.2
C(3)−C(2)−N(2)	121.7	121.6	121.1	120.6 (2.5)	121.0
O(3)−C(3)−C(2)	118.2	118.2	118.0	118.0 (2.6)	117.7
O(3)−C(3)−N(3)	119.9	119.9	120.1	120.3 (3.0)	118.9
C(2)−C(3)−N(3)	121.8	121.8	121.7	122.1 (3.2)	123.3
C(1)−N(1)−H(1)	119.3	119.1	117.7	117.5 (4.3)	116.1
C(1)−N(1)−H(2)	119.3	119.2	120.9	119.7 (4.7)	121.5
H(1)−N(1)−H(2)	121.3	121.4	121.3	120.2 (4.9)	122.3
O(21)−N(2)−O(22)	119.5	119.4	120.0	119.9 (2.5)	120.0
O(21)−N(2)−C(2)	120.6	120.9	119.4	119.6 (2.7)	120.0
O(22)−N(2)−C(2)	119.8	119.7	120.4	120.3 (2.7)	119.9
C(3)−N(3)−H(3)	121.3	121.9	119.2	119.5 (4.6)	120.1
C(3)−N(3)−H(4)	118.0	118.1	120.3	119.4 (4.7)	119.4
H(3)−N(3)−H(4)	120.6	120.0	120.0	118.4 (4.7)	120.5
N(2)−O(21)···H(2)	109.9	109.5	110.7	109.8 (3.7)	111.3
N(2)−O(22)···H(4)	109.2	109.4	109.5	108.8 (3.7)	110.3
N(1)−H(2)···O(21)	125.3	125.3	121.0	123.5 (7.1)	122.3
N(3)−H(4)···O(22)	129.1	128.9	126.7	126.3 (7.5)	125.8

[a]Bond lengths are in angstroms, angles in degrees. [b]With London-type empirical correction for dispersion interactions as proposed by Grimme. [c]From ref 34.

parameters) and vibrational harmonic and anharmonic frequency calculations were carried out on the level of PBE functional[46] with the two shrinking factors (5, 5) to generate a commensurate grid of *k*-points in reciprocal space, according to the Monkhorst−Pack method.[47] Additional calculations were carried out with inclusion of the London-type empirical correction for dispersion interactions (PBE+D) as proposed by Grimme.[48] The following basis sets were used in these studies: the 6-31d1G basis set for carbon, nitrogen, oxygen and 3-1p1G for hydrogen.[49] Vibrational frequency calculations in CRYSTAL09 were performed at the Γ-point.[22,44]

Molecular dynamics simulations have been carried out using the CPMD program version 3.13.2,[50] with the initial molecular configuration for the nitromalonamide crystal optimized by the

dx.doi.org/10.1021/jp312473b | J. Phys. Chem. B XXXX, XXX, XXX−XXX

preconditioned conjugate gradient (PCG) method with periodic boundary conditions (PBCs) employed for the solid state calculations. In these cases, real space Ewald summation of electrostatic interactions was carried out taking into account 8 cell replicas in each direction. The crystal data from the neutron diffraction study by Madsen[34] et al. have been selected as a starting point. The crystal is orthorhombic ($P2_12_12_1$) with cell dimensions a = 4.842, b = 4.967, c = 21.899 Å, and $\alpha = \beta = \gamma$ = 90° with four formula units in the unit cell (Z = 4).[34] Molecular dynamics and path integral simulations (NVT ensemble) were carried out at 298 K with a time step of 3.0 au (0.072566 fs), coupled to a Nosé−Hoover chain thermostat[51] at a frequency of 3200 cm^{-1}. An electronic mass parameter of 400 au was employed. Electronic exchange and correlation have been modeled using the gradient-corrected functional of Perdew, Burke, and Ernzerhof (PBE).[46] Core electrons were treated using the norm-conserving atomic pseudopotentials (PP) of Troullier and Martins,[52] while valence electrons were represented in a plane-wave basis set truncated at an extended energy cutoff of 70 Ry. Following the initial equilibration period, data was accrued for a further 45 ps for Car−Parrinello and imaginary-time (45 ps) for the path integral dynamics simulation, respectively for ten (PI10) Trotter replicas (polymer-beads) using the normal mode variable transformation. The data was visualized using the CHEMCRAFT[53] and VMD[54] programs, with the path integral data first processed using a script by Kohlmeyer to calculate the centroid position of each set of polymer-beads.[55]

The vibrational spectrum has been also calculated using the Fourier transformation of the dipole autocorrelation function obtained from dipole trajectories generated by the CPMD simulation facilitated by the scripts of Forbert and Kohlmeyer.[56]

RESULTS AND DISCUSSION

Let us first consider the results of full geometry optimization of NMA crystal by means of the CRYSTAL09 computer code.[44,45] Optimized and selected geometrical parameters together with the unit cell parameters on the DFT level with the PBE and PBE+D functionals are listed in Table 1 whereas the structure is presented in Figure 1. The reliability of the obtained results can be confirmed by comparison with the experimental data for the crystal published by Madsen and co-workers.[34] All calculations correctly predict that the shortest intramolecular hydrogen bond is O1−H(X)···O3. Moreover, contrary to the previous ab initio calculations of NMA molecule in the gas phase[29,34,35] where two symmetrical minima were localized for the O−H···O positions, for the crystal is observed only one asymmetrical intramolecular O−H···O hydrogen bond. In order to confirm that only one minimum for the strong O−H···O hydrogen bond exists on the potential energy surface, the bridging H(X) atom was moved into close contact to the O3 atom. After the full geometry optimization of a crystal, the bridging hydrogen atom was moved back to the vicinity of O1 atom, which supports that on the PES for the crystal is noted only asymmetrical O1−H(X)···O3 intramolecular hydrogen bond.

As one can expect, the dispersion correction has no influence on the chemical bonds. The most important influence of dispersion forces is on the value of unit cell parameters as is presented in Table 1. Whereas for a and b unit cell parameters the dispersion correction is not important, a completely different picture is observed for the c parameter. For calculations with PBE density functional the value of the c parameter (23.909 Å) is too large in comparison with the experimental value of 21.899 Å.[34] Inclusion in the density functional empirical dispersion correction gives a calculated value (21.389 Å) in very good agreement with experimental data. The large influence of the dispersion term on the c-axis parameter is probably due to the crystal structure of NMA because the ribbons of almost coplanar molecules form layers parallel to the ab plane.

In Table 1 are also presented selected structural geometrical parameters optimized by athermal geometry (PCG) from CPMD calculations as well as the average geometrical parameters from the CPMD simulations. For all three, calculated intramolecular H-bonded geometrical parameters are in good agreement with experimental neutron diffraction data.[34] The data presented in Table 1 clearly indicate that the O1−H(X)···O3 bond length is much shorter than the two other (N1−H2···O21, N3−H4···O22) intramolecular hydrogen bonds. Moreover, all calculations reproduce correctly the nonlinearity of all three intramolecular H-bonds.

The time evolution behavior of the bond lengths directly involved in intramolecular hydrogen bonds at 298 K is presented in Figure 2. First of all, the motion of protons in all three intramolecular H-bonds is not coupled. Analysis of the strong O1−H(X)···O3 intramolecular hydrogen bond shows a very large fluctuation of the bridging proton between two oxygen atoms (Figure 2a). It means that this proton is very mobile and it is delocalized in the O1−H(X)···O3 bridge. Moreover, the proton motion in this bridge is coupled with so-called slow O1···O3 motion. The O1−H(X) bond length changes in the range 1.10−1.3 Å in the CPMD simulations. Moreover, relatively large amplitude motion is noted for the O1···O3 distance (2.3−2.55 Å). For two intramolecular H-bonds N−H···O (N1−H2···O21, N3−H4···O22), the time evolution picture observed for the N1−H2 and H2···O21, also N3−H4 and H4···O22, respectively, bond lengths is typical for weak H-bonds (Figures 2b and 2c). Very small amplitude motion is observed for bridging protons bounded to nitrogen atoms (N1, N3) whereas large amplitude motions are noted for the O···H and N···O bonds.

The asymmetry of the O1−H(X)···O3 hydrogen bond and significant delocalization of the bridging proton are additionally supported by the proton distribution function along the reaction coordinate obtained from CPMD and PIMD simulations and presented in Figure 3. Reaction coordinate is defined as the difference between the O1−HX and HX−O2 bond lengths for the intramolecular H-bond. The midpoint position of the proton in the O1−H(X)···O3 hydrogen bridge is described by reaction coordinate equal to zero. Relatively narrow peak and shift to O1 atom (by ca. 0.3 Å from the midpoint) is observed for the proton distribution derived from the CPMD simulations. Inclusion in the simulation of quantum effects (PIMD approach) shows large change in proton behavior. The proton distribution curve is much broader, and maximum is shifted toward the midpoint of the O1−H(X)···O3 H-bond (ca. 0.18 Å from the midpoint if the O···O bond). It clearly indicates the relatively large delocalization of the proton in this bridge.

The resonance-assisted character of the strong O1−H(X)···O3 intramolecular H-bond is visible in Figure 4 where are presented the plots of distribution functions of C1−O1 and C3═O3 bond lengths from CPMD and PIMD simulations. In fact, there is only a small difference between the positions of maximum of distribution for C1−O1 and C3═O3

dx.doi.org/10.1021/jp312473b | J. Phys. Chem. B XXXX, XXX, XXX−XXX

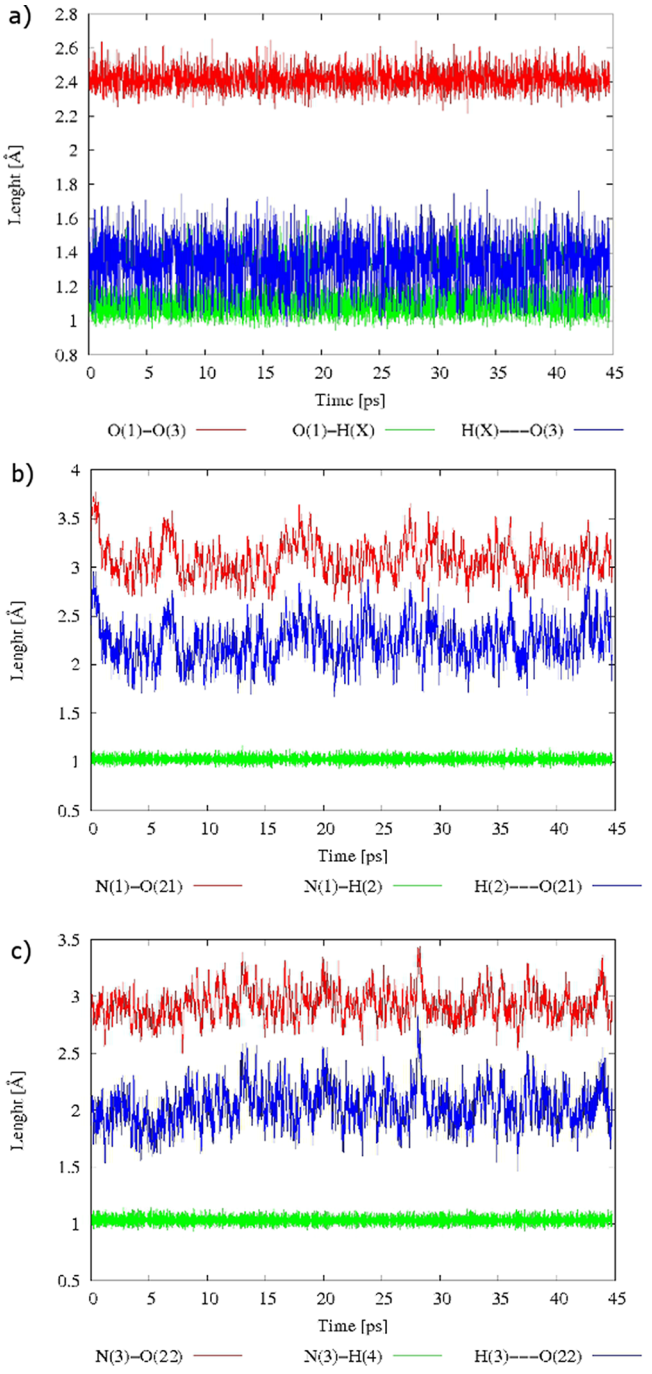

Figure 2. Time evolutions of the bonds involved in the three hydrogen bonds (a) O1-HX···O3, (b) N1–H2···O21, and (c) N3–H4···O22 from the CPMD calculations at 298 K.

bond lengths. It should be noted that the normal double and single bond lengths are 1.21 and 1.43 Å, respectively. In addition, an inspection of the C–C bond length presented in Table 1 clearly indicates a delocalization effect: some double character appears in single bonds and vice versa. Like for the proton distribution functions, the curves for carbon–oxygen bonds from the PIMD simulation are much broader than from the CPMD simulations. It means that the quantum effect plays also some role not only for the mobility in O1–H(X)···O3 intramolecular H-bond but also in the description of dynamics of heavy atoms.

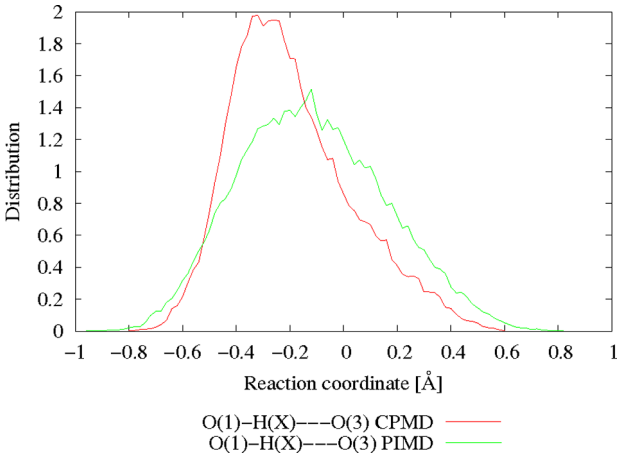

Figure 3. Distribution function of the protons from the CPMD and PIMD (10 beads) simulations at 298 K for the O1–HX···O3 hydrogen bond.

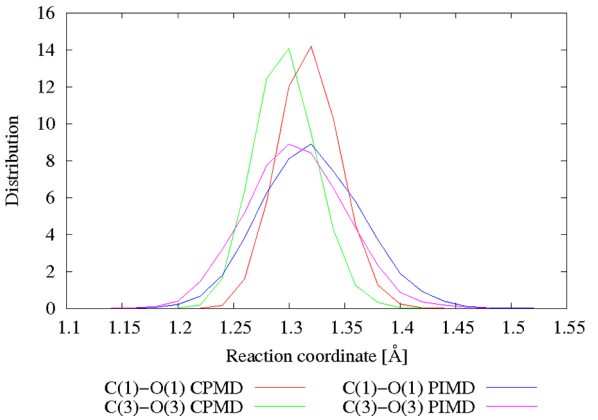

Figure 4. Distribution function of the length of the bonds C1–O1 and C3–O3 from the CPMD and PIMD (10 beads) simulations at 298 K.

Recently Omelchenko and co-workers have shown that the molecule with vicinal nitro and amino groups gives an opportunity for formation of RAHB between them.[57] Therefore it was interesting to analyze the resonance-assisted character of both weak intramolecular N–H···O hydrogen bonds. Very detailed analysis of data is presented in Table 1, and the time evolutions of bonds C1–N1, C2–N2, and C3–N3 received from the CPMD simulations (not shown here) do not indicate on the resonance-assisted character of those bonds.

Hydrogen-bonded systems are not rigid. Dynamics of proton motion in hydrogen bonds is also characterized by changes of other geometrical parameters related to hydrogen bridges. In Figure 5a are presented plots of distribution function of the O1–H(X)···O3, N1–H2···O21, and N3–H4···O22 angles for O–H···O and two N–H···O H-bonds whereas in Figure 5b are visible plots of distribution functions of C1–C2–C3 angle. Independently of the method of simulations, all presented distribution functions are relatively broad. It means that a relatively large change of this angle is noted during simulations by both methods (CPMD and PIMD). However it should be mentioned that the distribution functions received from the PIMD simulations are slightly broader than from the CPMD calculations. For example, the C1–C2–C3 angle changes from 108° to 129° in the PIMD simulations whereas the values from the CPMD simulations are in range 111–126°.

dx.doi.org/10.1021/jp312473b | J. Phys. Chem. B XXXX, XXX, XXX–XXX

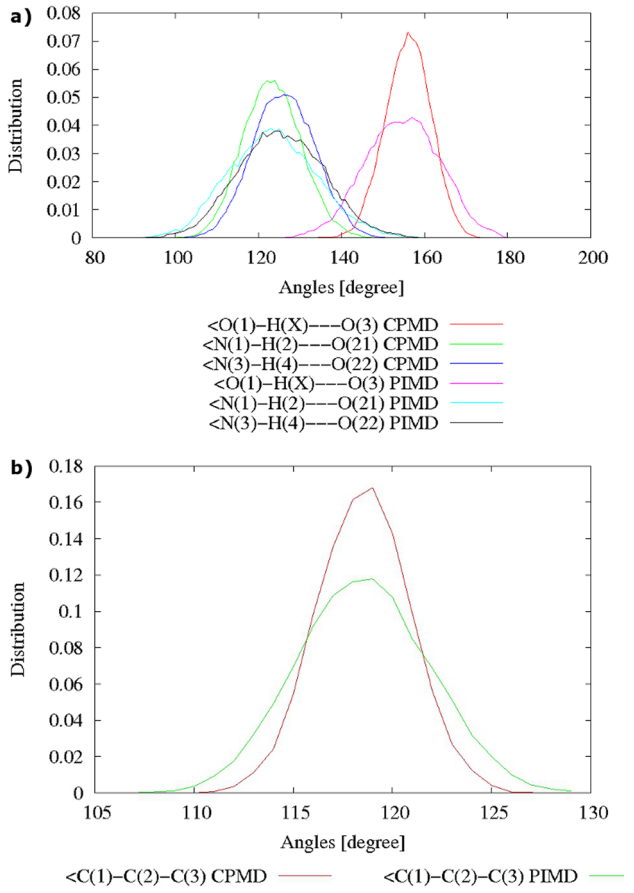

Figure 5. Distribution function of the angles for the three hydrogen bonds (a) O1–HX···O3, N1–H2···O21, N3–H4···O22 and distribution function of the angles for the bond (b) C1–C2–C3 from the CPMD and PIMD (10 beads) simulation at 298 K.

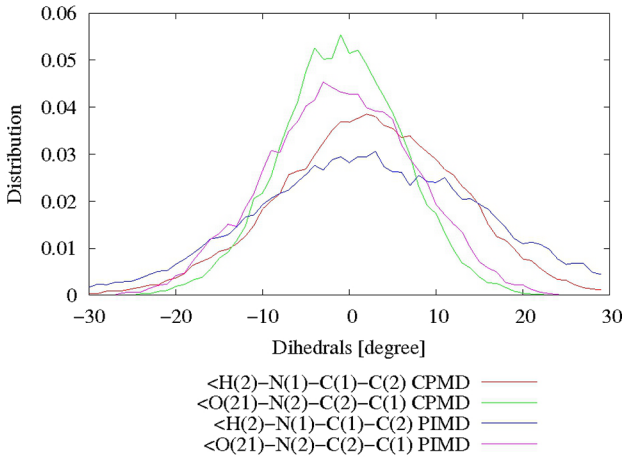

Figure 6. Distribution function of the dihedral angles: H2–N1–C1–C2 and O21–N2–C2–C1 from the CPMD and PIMD (10 beads) simulation at 298 K.

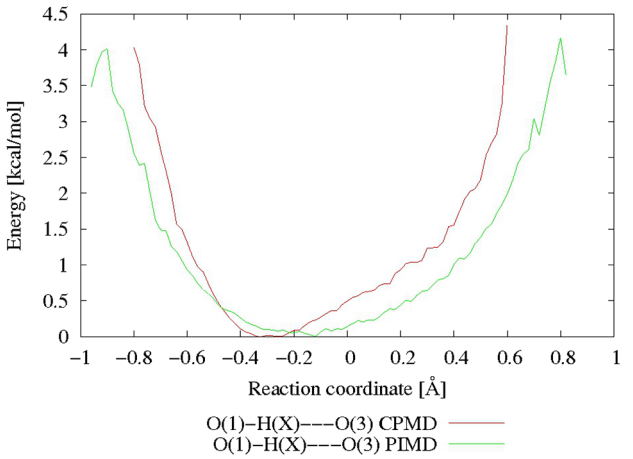

Figure 7. Free energy profile for proton motion in the O1–HX···O3 bond.

Very interesting is the influence of the NO_2 group on hydrogen bond strength in 2-nitromalonaldehyde. Buemi and Zuccurello[35] and Tayyari and co-workers[58] showed that the main effect on the NO_2 substituent is shortening of the O···O distance and lengthening of the O–H bond in comparison with corresponding values for unsubstituted malonaldehyde. On the other hand, by rotating the nitro group by 90° about C–N bond the O···O distance increased by about 0.05 Å.[58] In Figure 6 are presented the plots of distribution functions of two dihedral angles H2–N2–C1–C2 and O21–N2–C2–C1. They clearly indicate a very large amplitude motion of this fragment of molecule in the range from −30° to 30°. Moreover, it also means that both (N1–H2···O21, N3–H4···O22) H-bridges are not planar in a crystal. It also explains very large changes in the N···O and H···O bond lengths of both (N1–H2···O21, N3–H4···O22) H-bridges during simulations presented in Figures 2b and 2c. Moreover, it might suggest that there is a coupling between the nitro group rotation and the O1···O3 distance although it is very difficult to see this effect directly from the CPMD simulations.

One of the most important characteristics of the nature of hydrogen-bonded systems is a shape of the potential energy curve for the proton motion in the hydrogen bridge. Figure 7 shows the free energy profiles for the proton motion in the O1–H(X)···O3 hydrogen bond obtained from CPMD and PIMD results. Free energy profiles were calculated with eq 1:

$$\Delta F = -kT \ln[P(\delta)] \quad (1)$$

where k is the Boltzmann constant, T is the simulation temperature, and $P(\delta)$ is the proton distribution as a function of δ (the reaction coordinate). This parameter gives a measure of the degree of proton transfer within the hydrogen bond, with a value of zero indicating the midpoint of the hydrogen bridge. The profiles of the free energy in Figure 7 demonstrate the absence of effective barrier for proton transfer even without inclusion of quantum effects for the CPMD simulation. The quantum effects taken into account do not change the effective potential shape drastically. We observed one minimum potential shape in each case, but the profile of free energy obtained from CPMD is sharper and more asymmetrical than the profile from PIMD simulation, which accounts for the shape of proton distribution presented in Figure 3. Contrary to the previous gas-phase "static" ab initio calculations where symmetrical double well potential was noted,[29] the CPMD and PIMD simulations clearly indicate one single well and slightly asymmetric position of the proton in the strong O1–H(X)···O3 H-bond of the NMA crystal. For the PIMD simulations the minimum is very broad and slightly shifted to the midpoint of the hydrogen bond. It also indicated large mobility (or delocalization) of the proton in this H-bond.

dx.doi.org/10.1021/jp312473b | J. Phys. Chem. B XXXX, XXX, XXX–XXX

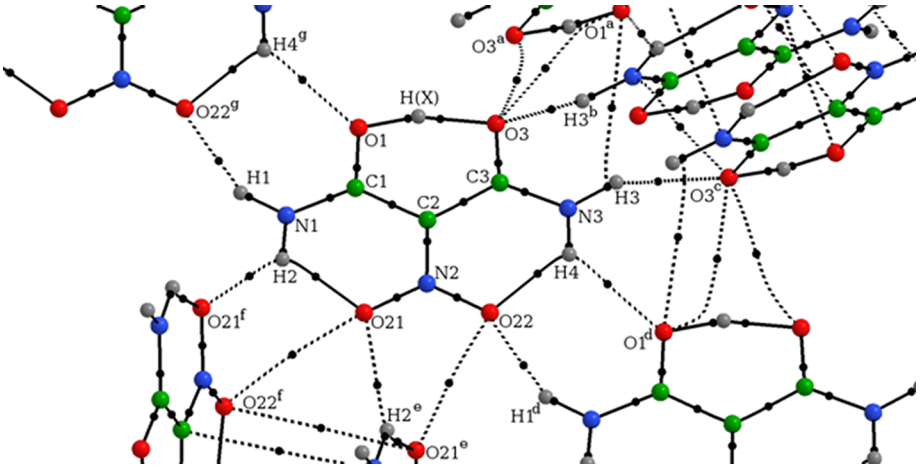

Figure 8. Molecular graphs for 8-molecular cluster of NMA crystal. The bond critical points are presented by small black circles whereas the dashed lines are the bond paths for intermolecular interactions.

Table 2. The Topological Properties of Selected Bond Critical Points (BCPs) Calculated for 8-Molecular Cluster at the B3LYP/cc-pVDZ Level[a]

BCP	atoms	$\rho(r)$	$\nabla^2\rho$	ε	H	V	E_{HB}[b]
			Intermolecular Interactions				
1	H3···O1[a]	0.0026	0.0137	1.1866	0.0009	−0.0016	−0.50
2	O3···H3[b]	0.0275	0.0900	0.0351	0.0012	−0.0201	−6.31
3	H3···O3[c]	0.0275	0.0901	0.0375	0.0012	−0.0201	−6.31
4	H4···O1[d]	0.0130	0.0423	0.0268	0.0004	−0.0098	−3.08
5	O1···H4[g]	0.0131	0.0421	0.0332	0.0004	−0.0098	−3.08
6	O22···H1[d]	0.0247	0.0923	0.0135	0.0023	−0.0186	−5.84
7	H1···O22[g]	0.0245	0.0930	0.0206	0.0024	−0.0185	−5.81
8	O21···H2[e]	0.0195	0.0594	0.0799	0.0002	−0.0145	−4.55
9	H2···O21[f]	0.0194	0.0599	0.0795	0.0002	−0.0146	−4.58
10	O3···O3[a]	0.0039	0.0187	2.9967	0.0010	−0.0027	
11	O3···O1[a]	0.0039	0.0201	4.0824	0.0011	−0.0029	
12	O22···O21[e]	0.0068	0.0294	0.3964	0.0007	−0.0059	
13	O21···O22[f]	0.0067	0.0295	0.5119	0.0008	−0.0058	
			Intramolecular Interactions				
14	O1−H(X)	0.2350	−0.8040	0.0119	−0.2868	−0.3727	
15	H(X)···O3	0.1186	0.0312	0.0170	−0.0764	−0.1606	−50.31
16	H2···O21	0.0351	0.1239	0.0235	0.0009	−0.0292	−9.16
17	H4···O22	0.0393	0.1396	0.0044	0.0008	−0.0333	−10.45

[a]All values are in au. Descriptions of bonds as in Figure 8. [b]Hydrogen bond strength (in kcal/mol) calculated from the formula E_{HB} = 0.5 V.

A very helpful and recognized method to study the nature of chemical bonds and intermolecular interactions is the quantum topological analysis of electron density by means of the quantum theory of atoms in molecules (QTAIM) method proposed by Bader.[43] The method allows the partition of a molecular space into atomic basins in terms of the topological properties of the electron density $\rho(r)$. The necessary conditions of existence of interaction between two atoms are the presence of a bond critical point (BCP) and the corresponding bond path (BP) linking their nuclei. A collection of all BPs in a molecule in its equilibrium geometry is called the molecular graph. The QTAIM is a very important and useful method especially for the characterization of the intra- and intermolecular H-bond interactions. It is worth mentioning that following characteristics of BCPs like the electron densities ρ_{BCP} and their Laplacians (∇^2_{BCP}) can be considered as a measure of H-bond strength.[19,59−67] Moreover, Rozas and co-workers[68] showed that both the Laplacian and the energy density (H_{BCP}) BCPs should also be used as the criteria to characterize hydrogen bonding interaction. For weak H-bonds (E_{HB} < 12.0) both $\nabla^2\rho_{BCP}$ and H_{BCP} > 0; medium H-bonds (12.0 < E_{HB} < 24.0 kcal/mol) show $\nabla^2\rho_{BCP}$ > 0 and H_{BCP} < 0; and for strong H-bonds (E_{HB} > 24.0 kcal/mol) both $\nabla^2\rho_{BCP}$ and H_{BCP} < 0. It should be mentioned that lately Mo raised a question of whether the QTAIM parameters are effective in the measure of H-bond strength.[69]

In order to characterize better all inter- and intramolecular hydrogen bonds existing in the NMA crystal we have applied the QTAIM method for a model cluster of 8 molecules with the crystal symmetry and geometrical structure of molecules in the crystal which is presented in Figure 8. Calculations for the cluster were performed using the Gaussian 09 version c01[70] package on the DFT level (B3LYP/cc-pVDZ). A topological analysis of $\rho(r)$ has been performed using the AIMAll[71] program. The results of the topological analysis of the electron density for selected bond critical points are presented in Table 2 whereas the molecular graphs and selected BCP for the studied cluster are displayed in Figure 8. The following

dx.doi.org/10.1021/jp312473b | J. Phys. Chem. B XXXX, XXX, XXX−XXX

topological parameters at BCPs are taken into consideration: the electron density (ρ), its Laplacian (∇^2), the energy density (H), the potential electron density (V), and ellipticity (ε). The topological properties of BCPs for intermolecular interactions presented in the upper part of Table 2 are characterized by the small value of the electron density, positive values of the Laplacian and the energy density. According to the criteria formulated by Rozas[61] and co-workers, these parameters belong to weak H-bond interactions and even more they are responsible for asymmetry of the O1−H(X)···O3 intramolecular H-bond. Therefore especially interesting are O1···H4^g and O3···H3^b intermolecular hydrogen bonds (see Figure 8). For both intermolecular H-bonds the Laplacian and energy density H at the BCPs are positive. However, the O3···H3^b hydrogen bond is stronger as is evident from the values of electron density ρ at the BCP (0.0275 au) and the Laplacian value of 0.0900 au in comparison to the O3···H3^b H-bond with values of electron density and Laplacian equal to 0.0131 au and 0.0421 au, respectively. Probably these intermolecular H-bonds are mainly responsible for the asymmetry of the O1−H(X)···O3 intramolecular H-bonds because both oxygen atoms of intramolecular H-bond participate as a proton acceptor in above-mentioned intermolecular H-bonds.

Another interesting issue is the topological analysis of the O1−H(X)···O3 strong intramolecular H-bonds presented in the bottom part of Table 2. For the O1−H(X) bond the Laplacian is negative as well as the energy density, H. As one can expect, this is the typical characteristic of a covalent bond. However, for the H(X)···O BCP the Laplacian value at the BCP is positive whereas the $H < 0$. It might suggest a medium strength H-bond, according to the Rozas et al. criteria[68] and with partial covalent character.

The last two lines in Table 2 present the topological characteristics of two intramolecular H-bonds (N1−H2···O21, N3−H4···O22) of NMA molecule in the crystal. The topological parameters indicated a relatively weak H-bond interaction (the electron density at the BCPs is relatively small, both the Laplacian and H are positive) which supports the conclusion formulated before on the basis of CPMD and PIMD simulations.

Contrary to intermolecular hydrogen bond energy calculations, estimation of the strength of intramolecular bonds is not trivial. One of the possibilities of estimation for this case is the calculation of the difference in energy between closed (X−H···Y) and open configuration.[72,73] Another possibility is application of isodesmic reaction: the H-bond energy is determined from suitable isodesmic reactions.[74] However, both methods of estimation of H-bond strength are possible for isolated systems in the gas phase where rotation of the X−H bond may occur but are not allowed for systems in a crystal.

Espinosa et al. showed that the H-bond energy may be correlated to the electronic potential energy density V at the H-bond critical point and E_{HB} as 0.5 V.[75] Calculated values of hydrogen bond strength (E_{HB}) from this formula are presented as the last column of Table 2. Estimated values of the intermolecular hydrogen bond energies look reasonable and are from −0.50 to H3···O1^a up to −5.81 kcal/mol for the H1···O22^g H-bond. The calculated value of E_{HB} for the O1−H(X)···O3 intramolecular H-bond equal to −50.41 kcal/mol is in our opinion greatly overestimated, similarly for both remaining N−H···O intramolecular H-bonds with E_{HB} equal −9.16 and −10.45 kcal/mol. Similar failure of the Espinosa et al. formula was previously observed for the C−H···O bonds in crystals.[76]

Grabowski proposed an estimation of the O−H···O intramolecular H-bond strength on the basis of relation between the intramolecular H-bond strength (E_{HB}) and the electron density at the H···O BCP and the H···O distance in malonaldehyde derivatives.[60] However, his considerations were restricted to the system with the E_{HB} smaller than −14 kcal/mol, which probably is out of scope for the O1−H(X)···O3 strong intramolecular H-bond in the NMA crystal. Therefore, for the estimation of this intramolecular H-bond we used the relation proposed by Musim and Marian:[27]

$$E_{HB} = (-5.554 \times 10^5) \exp(-4.12R) \quad (2)$$

where R is the O···O distance. Using the O1···O3 the average distance from the CPMD simulations (R = 2.419 Å), the calculated H-bond strength is equal to −26.1 kcal/mol and −29.4 kcal/mol for O1···O3 distance received for DFT optimization with Grimme correction. Taking into consideration three facts, that the formula 2 is an approximation as well as the results of H-bond strength obtained by Buemi and Zucarello for the isolated molecule in a gas phase is about 27 kcal/mol[35,36] and also relations of Rozas et al.[61] the base of QTAIM parameters are rather for ylide systems, we can suggest that the intramolecular O1−H(X)···O3 bond strength in the NMA crystal is ca. −27 kcal/mol. It means that this H-bond is very strong in the category of intramolecular hydrogen bonds.

Another way to characterize the H-bond interaction is the natural bond orbital (NBO) analysis.[77,78] The resonance-assisted mechanism H-bonds in the past were already studied by means of the NBO method,[16−18,27,67,79,80] so in this paper the analysis is concentrated to the study of all three intramolecular H-bonds in NMA. Weinhold shows that the charge transfer stabilization energy (ΔE_{CT}) is proportional to the hydrogen bond strength.[77] In Table 3 are presented the values of charge transfer stabilization energies and occupancies of NBOs responsible for intramolecular H-bonds but not for intermolecular H-bonds because they do not have an influence on resonance-assisted mechanism of intramolecular bond. All calculations were done for the single NMA molecule with the geometrical structure from crystal at the PBE/aug-cc-pVDZ level. NBO analysis shows that the two lone pairs of the O1 atom have contributed to the O1−H(X)···O3 intramolecular H-bond. Moreover, the values of charge transfer stabilization clearly show the stronger O1−H(X)···O3 H-bond whereas two N−H···O intramolecular bonds are much weaker. Comparison of σ^*_{O-H} and σ^*_{N-H} occupancies also confirms strong O1−H(X)···O(3) intramolecular H-bond. The results of NBO analysis are in qualitative agreement with the conclusions from the AIM data (see Table 2). The quantitative agreement between NBO and AIM approaches especially for the N1−H2···O21 and N3−H4···O22 H-bonds is not expected because

Table 3. Calculated Charge Transfer Stabilization Energies (ΔE_{CT}, in kcal/mol) and Occupancies (in e) of NBOs Responsible for Intramolecular H-Bonds

	ΔE_{CT}	orbital	occupancy	orbital	occupancy
$n_{1O3} \rightarrow \sigma^*_{O1-H(X)}$	11.12	n_{1O3}	1.96032	$\sigma^*_{O1-H(X)}$	0.16311
$n_{2O3} \rightarrow \sigma^*_{O1-H(X)}$	95.00	n_{2O3}	1.78764		
$n_{O21} \rightarrow \sigma^*_{N1-H2}$	11.62	n_{O21}	1.88957	σ^*_{N1-H2}	0.03534
$n_{O22} \rightarrow \sigma^*_{N3-H4}$	4.05	n_{O22}	1.97662	σ^*_{N3-H4}	0.03341

dx.doi.org/10.1021/jp312473b | J. Phys. Chem. B XXXX, XXX, XXX−XXX

Table 4. Calculated and Experimental Selected Vibrational Frequencies (in cm^{-1}) for the Nitromalonamide in the Solid State

	6-31d1G; 6-31d1; 3-1p1G					
	PBE		PBE+D[a]			
freq	harmonic	anharmonic	harmonic	anharmonic	CPMD/PBE/70 Ry	expt[b]
υNH asymm	3452	3142	3346	3170	3317	3400
υNH symm	3410	3130	3300	3120	3230	3290
υOH	2078	1551	2046	1528	1970	1870
δOH	1719		1705		1720	1696
δOH+υC═O	1709		1646		1680	1660
υC═O	1629		1607		1600	1648
δNH	1558		1560		1500	1510
υN═O	1538		1531		1490	1497
υN−O	1339		1333		1250	1296

[a]With London-type empirical correction for dispersion interactions as proposed by Grimme. [b]From ref 81.

the AIM analysis was done for a cluster of eight NMA molecules whereas the NBO calculations were performed for a single NMA molecule.

In the standard of ab initio calculations the vibrational frequencies are calculated at the harmonic level. In order to account anharmonic effects and other shortcomings usually the empirical scaling procedure is applied (e.g., refs 81−83). For strong hydrogen-bonded systems the anharmonicity is very important[84] and explicit incorporation of anharmonic effects in the theoretical approach is required.[85] In this paper the vibrational spectra of NMA crystal were calculated using Fourier transformation of the dipole autocorrelation function obtained for trajectories generated by CPMD simulations. Another significant advantage of this approach is that the anharmonic effects are included in all of vibrational modes and the crystal effect is taken into account. Selected vibrational frequencies from the CPMD simulations, together with harmonic and anharmonic frequencies from the static calculations of crystal and available experimental data[86] together with tentative assignments, are presented in Table 4. Figure 9 presents the calculated harmonic, CPMD, and experimental spectra of the NMA crystal. It can be seen that the CPMD simulated IR spectra reproduce correctly the complicated band shape observed in the experimental spectra of NMA as well as position of band maximum.[86] It should be noted that the CPMD IR spectrum reproduces vibrational frequencies much better than static DFT calculations for crystal in harmonic and anharmonic approach in comparison to the experimental data. For example, two very strong bands observed at 3317 and 3230 cm^{-1} (asymmetric and symmetric N−H stretching, respectively) in the CPMD spectra are in a very good accord with the experimental values of 3400 and 3290 cm^{-1}.[85] The most interesting finding for this paper is the O−H stretching mode. Analysis of the CPMD spectra localized it at 1970 cm^{-1}, which is in reasonable agreement with the experimental value (1870 cm^{-1}). In both spectra, i.e., theoretical and experimental, the intensity of the O−H stretching mode is very low and is almost invisible on both spectra in comparison to the other bands. However, very careful analysis of the CPMD spectra in the region of O−H stretching mode indicates a very broad band which is typical for the strong H-bonds. It is also important to note that the calculated anharmonic stretching frequencies by means of DFT approach and presented in Table 4 are greatly underestimated in comparison with CPMD and experimental spectra. One of the possible reasons for this estimation is the lack of coupling with other modes. In the case of the H-bond systems, for example, the O−H stretching mode is greatly coupled to the O···O stretching with so-called slow motion.[6] In our opinion the procedure of calculation of anharmonic stretching frequency presented in CRYSTAL09 program[44] is over-simplified.

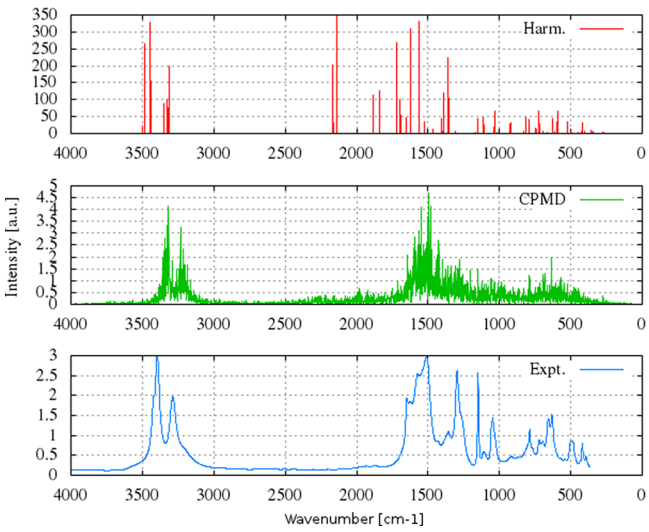

Figure 9. The comparison of the simulated IR spectra for the nitromalonamide in the solid state from the DFT (PBE) harmonic calculation with London-type empirical correction for dispersion interactions (upper), with CP molecular dynamics simulation at 298 K (middle), and experimental IR absorbance spectrum in KBr tablet (lower).[86].

CONCLUSION

In this paper are presented the results of theoretical studies on the intramolecular hydrogen bonds in nitromalonamide crystal. This molecule is an unusual example of a molecular system with three intramolecular hydrogen bonds of different bond strength. One of them, the O1−H(X)···O3, is very short and strong whereas the two remaining (N1−H2···O21, N3−H4···O22) hydrogen bonds are weak. The QTAIM analysis of topological parameters at BCP points clearly indicates strong interaction with some contribution of covalency in the O1−H(X)···O3 H-bond. The estimated H-bond strength based on the Musim and Marian relation[27] is equal to ca. −27 kcal/mol.

CPMD and static calculations at the DFT level with the PBE functional by means of the CRYSTAL program shows a good

dx.doi.org/10.1021/jp312473b | J. Phys. Chem. B XXXX, XXX, XXX−XXX

agreement of the optimized geometrical parameters with the previously published experimental structure.[34] However, for proper reproduction of lattice cell parameters it is necessary to include empirical dispersion correction to the PBE functional.

The presented results of both simulations at the CPMD and PIMD levels indicate a large degree of mobility of the proton in the very short O1−H(X)···O3 bond. A free energy profile, as well as the proton distribution in this intramolecular hydrogen bond, does not indicate a double well potential and it is not a tautomeric equilibrium as was previously suggested on the base of static gas-phase calculations. Moreover, we demonstrate that for the O1−H(X)···O3 hydrogen bond the proton is shared between two oxygen atoms and a very flat, slightly asymmetric potential energy is observed. The inclusion of quantum effects for nuclear motion, as is done in the PIMD simulation, plays an important role.

The Car−Parrinello molecular dynamics method proved to reproduce the band shape in the infrared spectra of NMA molecule in the solid state, which is in good agreement with experimental data.

AUTHOR INFORMATION

Corresponding Author

*E-mail: piotr@elrond.chem.uni.wroc.pl. Website: http://kwanty.wchuwr.pl/?q=durlak.

Notes

The authors declare no competing financial interest.

ACKNOWLEDGMENTS

The authors thank Dr. Andrzej Bil (Faculty of Chemistry, University of Wroclaw, Poland) for insightful discussions during the paper preparation as well as to Dr. Jens Spanget-Larsen (Department of Science, Roskilde University, Denmark) for sending the experimental IR spectra of NMA crystal. We also want to thank the Academic Computer Centre in Gdansk (CI TASK) for the use of the Galera-ACTION Cluster and the Wroclaw Centre for Networking and Supercomputing (WCSS) for the use of the Supernova Cluster.

REFERENCES

(1) *Intermolecular Interactions − From van der Waals to Strongly Bound Complexes*; Scheiner, S., Ed.; Wiley-Blackwell: New York, 1997.

(2) Desiraju, G. R.; T. Steiner., T. In *The Weak Hydrogen Bond in Structural Chemistry and Biology*; Oxford University Press: New York, 1999.

(3) Perrin, C. L.; Nielson, J. B. *Annu. Rev. Phys. Chem.* **1997**, *48*, 511−544.

(4) *Theoretical Treatment of Hydrogen Bonding*; Hadži, D., Ed.; Wiley: Chichester, 1997.

(5) Desiraju, G. R. *Acc. Chem. Res.* **2002**, *35*, 565−573.

(6) Elsaesser, T.; Bakker, H. J. In *Ultrafast Hydrogen Bonding Dynamics and Proton Transfer Processes in the Condensed Phase*; Kluwer Academic Publishers: Dordrecht, 2002.

(7) Sobczyk, L.; Grabowski, S. J.; Krygowski, T. M. *Chem. Rev.* **2005**, *105*, 3513−3560.

(8) *Hydrogen-Transfer Reactions*; Hynes, J. T., Klinman, J. P., Limbach, H.-H., Showen, R. L., Eds.; Wiley-VCH: Weinheim, 2007.

(9) Maréchal, Y. In *The Hydrogen Bond and the Water Molecule. The Physics and Chemistry of Water, Aqueous and Bio Media*; Elsevier: Amsterdam, 2007.

(10) Gilli, G.; Gilli, G. P. In *The Nature of the Hydrogen Bond*; Oxford University Press: Oxford, 2009.

(11) Gilli, G.; Bellucci, F.; Ferretti, V.; Bertolasi, V. *J. Am. Chem. Soc.* **1989**, *111*, 1023−1028.

(12) Bertolasi, V.; Gilli, P.; Ferretti, V.; Gilli, G. *J. Am. Chem. Soc.* **1991**, *113*, 4917−4925.

(13) Gilli, P.; Bertolasi, V.; Ferretti, V.; Gilli, G. *J. Am. Chem. Soc.* **1994**, *116*, 909−915.

(14) Gilli, P.; Bertolasi, V.; Pretto, L.; Ferretti, V.; Gilli, G. *J. Am. Chem. Soc.* **2004**, *126*, 3845−3855.

(15) Gilli, P.; Bertolasi, V.; Pretto, L.; Antonov, L.; Gilli, G. *J. Am. Chem. Soc.* **2005**, *127*, 4943−4953.

(16) Zubatyuk, R. I.; Volovenko, Y. M.; Shishkin, O. V.; Gorb, L.; Leszczynski, J. *J. Org. Chem.* **2007**, *72*, 725−735.

(17) Sanz, P.; Mo, O.; Yanez, M.; Elguerro, J. *J. Phys. Chem. A* **2007**, *111*, 3585−3591.

(18) Zubatyuk, R. I.; Shshkin, O. V.; Gorb, L.; Leszczynski. *J. Phys. Chem. A* **2009**, *113*, 2943−2952.

(19) Grabowski, S. J. *J. Phys. Org. Chem.* **2004**, *17*, 18−31.

(20) Lyssenko, K. A.; Antipin, M. Yu. *Russ. Chem. Bull.* **2006**, *55*, 1−15.

(21) Grabowski, S. J. *Annu. Rep. Prog. Chem., Sect. C* **2006**, *102*, 131−165.

(22) Grabowski, S. J.; Leszczynski, J. In *Hydrogen Bonding—New Insights*; Grabowski, S. J., Ed.; Springer: Berlin, 2006; pp 487−512.

(23) Hayashi, T.; Mukamel, S. *J. Phys. Chem. A* **2003**, *107*, 9113−9131.

(24) Fillaux, F.; Nicolai, B. *Chem. Phys. Lett.* **2005**, *416*, 357−361.

(25) Caminati, W.; Grabow, J. U. *J. Am. Chem. Soc.* **2006**, *128*, 854−857.

(26) Zhao, X.; Rossi, P.; Barsegov, V.; Zhou, J.; Woodford, J. N.; Harbison, G. S. *J. Mol. Struct.* **2006**, *790*, 152−159.

(27) Musin, R. N.; Mariam, Y. H. *J. Phys. Org. Chem.* **2006**, *19*, 425−444.

(28) Woodford, J. N. *J. Phys. Chem. A* **2007**, *111*, 8519−8530.

(29) Hargis, J. C.; Evangelista, F. A.; Ingels, J. B.; Schaefer, H. F., III *J. Am. Chem. Soc.* **2008**, *130*, 17471−17478.

(30) Bertolasi, V.; Ferretti, V.; Gilli, P.; Yao, X.; Li, C. -J. *New J. Chem.* **2008**, *32*, 694−704.

(31) Zarycz, N.; Aucar, G. A.; Vedova, C. O. D. *J. Phys. Chem. A* **2010**, *114*, 7162−7172.

(32) Belova, N. V.; Girichev, G. V.; Oberhammer, H.; Hoang, T. N.; Shlykov, S. A. *J. Phys. Chem. A* **2012**, *116*, 3428−3435.

(33) Simonsen, O.; Thorup, N. *Acta Crystallogr., Sect. B* **1979**, *35*, 432−435.

(34) Madsen, G. K. H.; Wilson, C.; Nymand, T. M.; McIntyre, G. J.; Larsen, F. K. *J. Phys. Chem. A* **1999**, *103*, 8684−8690.

(35) Buemi, G.; Zuccarello, F. *Chem. Phys.* **2004**, *306*, 115−129.

(36) Buemi, G.; Zuccarello, F. *J. Mol. Struct. THEOCHEM* **2005**, *719*, 137−148.

(37) Hansen, P. E. *Magn. Reson. Chem.* **2008**, *46*, 726−729.

(38) Sebban, M.; Gullard, J.; Palmas, P.; Poullain, D. *Magn. Reson. Chem.* **2005**, *43*, 563−566.

(39) Car, R.; Parrinello, M. *Phys. Rev. Lett.* **1985**, *55*, 2471−2474.

(40) Marx, D.; Parrinello, M. *Z. Phys., Sect. B* **1994**, *95*, 143−144.

(41) Marx, D.; Parrinello, M. *J. Chem. Phys.* **1996**, *104*, 4077−4082.

(42) Tuckerman, M.; Marx, D.; Klein, M. L.; Parrinello, M. *J. Chem. Phys.* **1996**, *104*, 5579−5588.

(43) Bader, R. F. W. In *Atoms in Molecules: A Quantum Theory*; Oxford University Press: Oxford, 1990.

(44) Dovesi, R.; Saunders, V. R.; Roetti, C.; Orlando, R.; Zicovich-Wilson, C. M.; Pascale, F.; Civalleri, B.; Doll, K.; Harrison, N. M.; Bush, I. J.; D'Arco, Ph.; Llunell, M.; Torino *CRYSTAL09 User's Manual*; University of Torino: 2009.

(45) Dovesi, R.; Orlando, R.; Civalleri, B.; Roetti, C.; Saunders, V. R.; Zicovich-Wilson, C. M. *Z. Kristallogr.* **2005**, *220*, 571−573.

(46) Perdew, P.; Burke, K.; Ernzerhof, M. *Phys. Rev. Lett.* **1996**, *77*, 3865−3868.

(47) Monkhorst, J.; Pack, J. D. *Phys. Rev.* **1976**, *13*, 5188−5192.

(48) Grimme, S. *J. Comput. Chem.* **2006**, *27*, 1787−1799.

(49) Gatti, C.; Saunders, V. R.; Roetti, C. *J. Chem. Phys.* **1994**, *101*, 10686−10696.

(50) CPMD, version 3.13.2; Copyright IBM Corp 1990−2008, Copyright MPI für Festkörperforschung Stuttgart 1997−2001; http://www.cpmd.org.
(51) Martyna, G. J.; Klein, M. L.; Tuckerman, M. *J. Chem. Phys.* **1992**, *97*, 2635−2643.
(52) Troullier, N.; Martins, J. L. *Phys. Rev.* **1991**, *B43*, 1993−2006.
(53) ChemCraft, http://www.chemcraftprog.com.
(54) Humphrey, W.; Dalke, A.; Schulten, K. *J. Mol. Graphics* **1996**, *14*, 33−38.
(55) Kohlmeyer, A.; Forbert, H. *traj2xyz.pl, version 1.4*; 2004.
(56) Forbert, H.; Kohlmeyer, A. *Fourier, version 2*; 2002−05.
(57) Omelchenko, I. V.; Shishkin, O. V.; Gorb, L.; Hill, F. C.; Leszczynski, J. *Struct. Chem.* **2012**, *23*, 1585−1597.
(58) Tayyari, S. F.; Moosavi-Tekyen, Z.; Zahedi-Tabrizi, M.; Eshghi, H.; Emampour, J. S. *J. Mol. Struct. THEOCHEM* **2006**, *782*, 191−199.
(59) Grabowski, S. J. *J. Phys. Chem. A* **2001**, *105*, 10739−10746.
(60) Grabowski, S. J. *J. Mol. Struct.* **2001**, *562*, 137−143.
(61) Rozas, I. *Phys. Chem. Chem. Phys.* **2007**, *9*, 2782−2790.
(62) Grabowski, S. J. *Chem. Rev.* **2011**, *111*, 2597−2625.
(63) Schmidtmann, M.; Farrugia, L. J.; Middlemis, D. S.; Gutmann, M. J.; McIntyre, G. J.; Wilson, C. C. *J. Phys. Chem. A* **2009**, *113*, 13985−13997.
(64) Grabowski, S. *J. Phys. Org. Chem.* **2003**, *16*, 797−802.
(65) Grabowski, S. *Annu. Rep. Prog. Chem.* **2006**, *102*, 131−165.
(66) Małecka, M. *J. Mol. Struct.* **2007**, *831*, 135−143.
(67) Nowroozi, A.; Raissi, H.; Hajiabadi, H.; Mohammadzadeh Jahani, P. *Int. J. Quantum Chem.* **2011**, *111*, 3040−3047.
(68) Rozas, I.; Alkorta, I.; Elguero, J. *J. Am. Chem. Soc.* **2000**, *122*, 11154−11161.
(69) Mo, Y. *J. Phys. Chem.* **2012**, *116*, 5240−5246.
(70) Frisch, M. J.; Trucks, G. W.; Schlegel, H. B.; Scuseria, G. E.; Robb, M. A.; Cheeseman, J. R.; Scalmani, G.; Barone, V.; Mennucci, B.; Petersson, G. A.; Nakatsuji, H.; Caricato, M.; Li, X.; Hratchian, H. P.; Izmaylov, A. F.; Bloino, J.; Zheng, G.; Sonnenberg, J. L.; Hada, M.; Ehara, M.; Toyota, K.; Fukuda, R.; Hasegawa, J.; Ishida, M.; Nakajima, T.; Honda, Y.; Kitao, O.; Nakai, H.; Vreven, T.; Montgomery, Jr., J. A.; Peralta, J. E.; Ogliaro, F.; Bearpark, M.; Heyd, J. J.; Brothers, E.; Kudin, K. N.; Staroverov, V. N.; Kobayashi, R.; Normand, J.; Raghavachari, K.; Rendell, A.; Burant, J. C.; Iyengar, S. S.; Tomasi, J.; Cossi, M.; Rega, N.; Millam, J. M.; Klene, M.; Knox, J. E.; Cross, J. B.; Bakken, V.; Adamo, C.; Jaramillo, J.; Gomperts, R.; Stratmann, R. E.; Yazyev, O.; Austin, A. J.; Cammi, R.; Pomelli, C.; Ochterski, J. W.; Martin, R. L.; Morokuma, K.; Zakrzewski, V. G.; Voth, G. A.; Salvador, P.; Dannenberg, J. J.; Dapprich, S.; Daniels, A. D.; Farkas, Ö.; Foresman, J. B.; Ortiz, J. V.; Cioslowski, J.; Fox, D. J. *Gaussian 09, Revision c01*; Gaussian, Inc.: Wallingford, CT, 2009.
(71) Keith, T. A.; *AIMAll (Version 10.05.04)*; TK Gristmill Software: Overland Park, KS, 2010 (http://aim.tkgristmill.com).
(72) Latajka, Z.; Scheiner, S. *J. Phys. Chem.* **1992**, *96*, 9764−9767.
(73) Luth, K.; Scheiner, S. *J. Phys. Chem.* **1994**, *98*, 3582−3887.
(74) Rozas, I.; Alkorta, I.; Elguero, J. *J. Phys. Chem. A* **2001**, *105*, 10462−10467.
(75) Espinosa, E.; Molins, E.; Lecomte, C. *Chem. Phys. Lett.* **1998**, *285*, 170−173.
(76) Gatti, C.; May, E.; Destro, R.; Cargnoni, F. *J. Phys. Chem. A* **2002**, *106*, 2707−2720.
(77) Weinhold, F. *J. Mol. Struct. THEOCHEM* **1997**, *398*−*399*, 181−197.
(78) Weinhold, F.; Landis, C. R. In *Discovering Chemistry with Natural Bond Orbitals*; Wiley: 2012.
(79) Pakiari, A. H.; Eskandari, K. *J. Mol. Struct. THEOCHEM* **2006**, *759*, 51−60.
(80) Rozas, I. *Phys. Chem. Chem. Phys.* **2007**, *9*, 2782−2790.
(81) Halls, M. D.; Velkovsky, J.; Schlegel, H. B. *Theor. Chem. Acc.* **2001**, *105*, 413−421.
(82) Johnson, R. D., III; Irikura, K. K.; Kacker, R. N.; Kessel, R. *J. Chem. Theory Comput.* **2010**, *6*, 2822−2828.
(83) Bauschlicher, C. W. *Mol. Phys.* **2010**, *108*, 2647−2654.
(84) Bratos, S.; Leicknam, J. -Cl.; Gallot, G.; Ratajczak, H. In *Ultrafast Hydrogen Bonding Dynamics and Proton Transfer Processes in the Condensed Phase*; Elsaesser, T., Bakker, H. J., Eds.; Kluwer Academic Publishers: Dordrecht, 2002; pp 5−30.
(85) Lüttschwager, N. O. B.; Wassermann, T. N.; Coussan, S.; Suhm, M. A. *Phys. Chem. Chem. Phys.* **2010**, *12*, 8201−8207.
(86) Spanget-Larsen, J.; Hansen, B. K. V.; Hansen, P. E. *Chem. Phys.* **2011**, *389*, 107−115.